AGU PUBLICATIONS

JGR

Journal of Geophysical Research: Space Physics

RESEARCH ARTICLE
10.1002/2016JA023335

Special Section:
Geospace system responses to the St. Patrick's Day storms in 2013 and 2015

Key Points:
- Different types of broad plasma depletions (BPDs) were detected during the 2015 St. Patrick's Day (17 March) storm
- BPDs of gradual and steep density gradient were detected in the longitudes where bubbles were absent and present, respectively
- Ionospheric uplift was responsible for the BPDs, but the spatial discontinuity caused by bubbles made steep walls of the BPDs

Correspondence to:
H. Kil,
hyosub.kil@jhuapl.edu

Citation:
Kil, H., W. K. Lee, L. J. Paxton, M. R. Hairston, and G. Jee (2016), Equatorial broad plasma depletions associated with the evening prereversal enhancement and plasma bubbles during the 17 March 2015 storm, *J. Geophys. Res. Space Physics*, *121*, 10,209–10,219, doi:10.1002/2016JA023335.

Received 15 AUG 2016
Accepted 28 SEP 2016
Accepted article online 29 SEP 2016
Published online 13 OCT 2016

Equatorial broad plasma depletions associated with the evening prereversal enhancement and plasma bubbles during the 17 March 2015 storm

Hyosub Kil[1], Woo Kyoung Lee[2], Larry J. Paxton[1], Marc R. Hairston[3], and Geonhwa Jee[4]

[1]The Johns Hopkins University Applied Physics Laboratory, Laurel, Maryland, USA, [2]Korea Astronomy and Space Science Institute, Daejeon, South Korea, [3]Physics Department, University of Texas at Dallas, Richardson, Texas, USA, [4]Korea Polar Research Institute, Incheon, South Korea

Abstract Broad plasma depletions (BPDs) in the equatorial *F* region represent plasma depletions whose longitudinal and latitudinal scales are much greater than those of normal plasma bubbles. This study investigates the characteristics and origin of BPDs using the coincident ionospheric observations by the Communication/Navigation Outage Forecasting System, Defense Meteorological Satellite Program, and Swarm satellites during the 2015 St. Patrick's Day (17 March) storm. Two types of BPDs were detected before midnight during the main phase of the storm. One type of BPDs showed a gradual plasma density variation (Type 1), and the other type of BPDs showed a steep density gradient (Type 2) at the walls of BPDs. The Type 1 BPDs were detected with no signature of plasma bubbles nearby, whereas the Type 2 BPDs were accompanied by bubbles. The formation of the Type 1 BPDs is attributed to the uplift of the bottomside of the *F* region above the satellite altitude by the action of storm-induced electric fields. The steep walls of Type 2 BPDs are associated with the ionospheric uplift and the spatial discontinuity of the ionosphere produced by bubbles. The detection of BPDs that are more than 15° wide in latitude by the polar orbit Swarm satellites arises from the elongation of bubbles along the magnetic field lines and the alignment of the elongation with the plane of the orbit.

1. Introduction

One of the many fascinating phenomena in the ionosphere during large geomagnetic storms is the abnormally large plasma depletions that occur at night in the equatorial *F* region. Plasma depletions of a few degrees in longitude (we call them plasma bubbles) frequently occur in the equatorial *F* region regardless of whether there are storms or not, but larger-scale and deeper plasma depletions have been preferentially observed during large geomagnetic storms. We call them broad plasma depletions (BPDs) to distinguish them from the more usual ionospheric bubbles. BPDs seem to occur in association with large storms, and their creation mechanism is considered to be different from the creation mechanism of bubbles. BPDs are the phenomena identified by in situ satellite observations [*Basu et al*., 2001, 2007; *Burke et al*., 2000, 2009; *Greenspan et al*., 1991; *Huang et al*., 2011; *Kil and Paxton*, 2006; *Kil and Lee*, 2013; *Kil et al*., 2006; *Lee et al*., 2014; *Su et al*., 2002].

The creation of plasma bubbles is well understood in terms of the concept of the "rising bubble" [*Woodman and La Hoz*, 1976]. The perturbation of the height or density in the bottomside of the *F* region grows to the topside by the generalized Rayleigh-Taylor instability [e.g., *Kelley*, 2009; *Sultan*, 1996]. The detection of the bottomside low-density plasma at higher altitudes appears as a plasma depletion or bubble. The detection of BPDs can also be understood in terms of the vertical transport of bottomside plasma. BPDs appear in satellite observations when the whole *F* region is lifted above the satellite orbits by storm-induced electric fields [*Basu et al*., 2001, 2007; *Greenspan et al*., 1991; *Kil and Lee*, 2013; *Lee et al*., 2014; *Su et al*., 2002]. A spike-like increase in the vertical plasma motion has been observed at premidnight during large geomagnetic storms, and this phenomenon was attributed to the intensification of the evening prereversal enhancement (PRE) by storm-induced electric fields [e.g., *Kil et al*., 2007, 2008; *Ramsingh et al*., 2015]. The formation of BPDs is also explained by the development of abnormally large bubbles by storm-induced electric fields [*Burke et al*., 2000] or by the accretion of normal bubbles [*Huang et al*., 2011; *Kil and Paxton*, 2006]. The development of abnormally large bubbles is supported by the observation of the large vertical plasma

velocity [*Burke et al*., 2000], and the accretion of bubbles is supported by model simulations [*Huang et al*., 2012; *Huba et al*., 2015].

This report investigates the characteristics and origin of BPDs by analyzing coincident satellite observations during the 2015 St. Patrick's Day (17 March) storm. *Tulasi Ram et al*. [2016] reported the detection of severe plasma depletions in the Indian sector by the Swarm and Communication/Navigation Outage Forecasting System (C/NOFS) satellites during the storm. The depletions were detected at the evening terminator, and these phenomena were attributed to the uplift of the *F* region above the satellite altitudes by the penetration electric field. The existence of a significant ionospheric uplift was supported by the ionosonde observations in India [*Ramsingh et al*., 2015; *Tulasi Ram et al*., 2016]. In addition to the BPDs in the Indian sector reported by *Tulasi Ram et al*. [2016], we have identified the occurrence of BPDs in two other longitude regions during the 2015 St. Patrick's Day storm. BPDs occurred in the longitudes where bubbles were absent as well as in the longitudes where bubbles were present. Two different types of BPDs occurred: Type 1 BPDs had a gradual density variation and Type 2 BPDs had a steep density gradient at the walls. The Type 1 BPDs did not accompany bubbles, whereas Type 2 BPDs accompanied bubbles. These observations provide a useful tool for the understanding of the origin of BPDs, especially the association of BPDs with bubbles. BPDs were detected between 18 and 22 h local times (LTs). This is the LT region where PRE and bubbles develop. During the 17 March 2015 storm, Swarm and Defense Meteorological Satellite Program (DMSP) satellite observations were available in this LT region. C/NOFS orbits were close to the magnetic equator in the longitudes where BPDs were detected. We can definitively investigate the ionospheric conditions at the times of the BPD detection using multiple satellite observations.

The observation data are described in section 2. Ionospheric observations in three different longitude regions are presented separately in section 3. We discuss the morphology of BPDs and its dependence on the satellite pass in section 4. Conclusions are given in section 5.

2. Data Description

C/NOFS mission was sponsored by the Air Force of the United States for the investigation of the turbulence in the equatorial ionosphere and its effect on communication and navigation systems [*de La Beaujardière and the C/NOFS Definition Team*, 2004]. The C/NOFS satellite was launched on 16 April 2008 and ended on 28 November 2015. The satellite had a nominal elliptical (400–800 km) orbit with an orbital inclination of 13°. The Coupled Ion Neutral Dynamic Investigation, one of the C/NOFS payloads, was sponsored by National Aeronautics and Space Administration and was composed of two instruments: Ion Velocity Meter (IVM) and Neutral Wind Meter (NWM). IVM measured the temperature, velocity, and concentration of charged particles, and NWM measured the velocity of neutral particles [*Heelis et al*., 2009]. This study uses the IVM measurements of the ion concentration with 1 s time resolution. We also present the meridional (vertical) ion velocity derived from the IVM measurements, but they are used as supporting material because the final version of the data products has not yet been produced. The C/NOFS orbit decayed to an elliptical orbit with the perigee of 350 km and apogee of 514 km on 17 March 2015.

The DMSP spacecraft are managed by the United States Air Force. They have Sun-synchronous circular orbits (inclination: 98°) at an altitude of approximately 830 km. F18 and F19 were launched on 18 October 2009 and 2 April 2014, respectively. The LTs of the northbound F18 and F19 ground tracks at the equator are 19.6 and 18.6 h, respectively. This study uses the measurements of the ion concentration and vertical ion velocity by the Special Sensors Ions, Electrons, and Scintillation (SSIES) sensor. The cadence rate of the SSIES data is 1 s. We also use the optical observation of the ionosphere by the Special Sensor Ultraviolet Spectrographic Imager (SSUSI) [*Paxton et al*., 1992a, 1992b] on board DMSP F18. SSUSI measures ultraviolet emissions in five different wavelength bands (HI 121.6 nm, OI 130.4 nm, OI 135.6 nm, and N_2 Lyman-Birge-Hopfield short and long (167.2 to 181.2 nm)) from the Earth's upper atmosphere. The OI 135.6 nm emission at night is produced by the recombination of oxygen ions and their subsequent de-excitation. Therefore, the intensity of OI 135.6 nm emission is a measure of the line-of-sight integral of the *F* region plasma density. The disk-scan OI 135.6 nm image is used for the investigation of the ionospheric morphology and the occurrence of bubbles.

The Swarm mission is sponsored by the European Space Agency for an accurate measurement of the Earth's magnetic field [*Lühr et al*., 2015]. Swarm consists of three circular-orbit satellites and was launched on

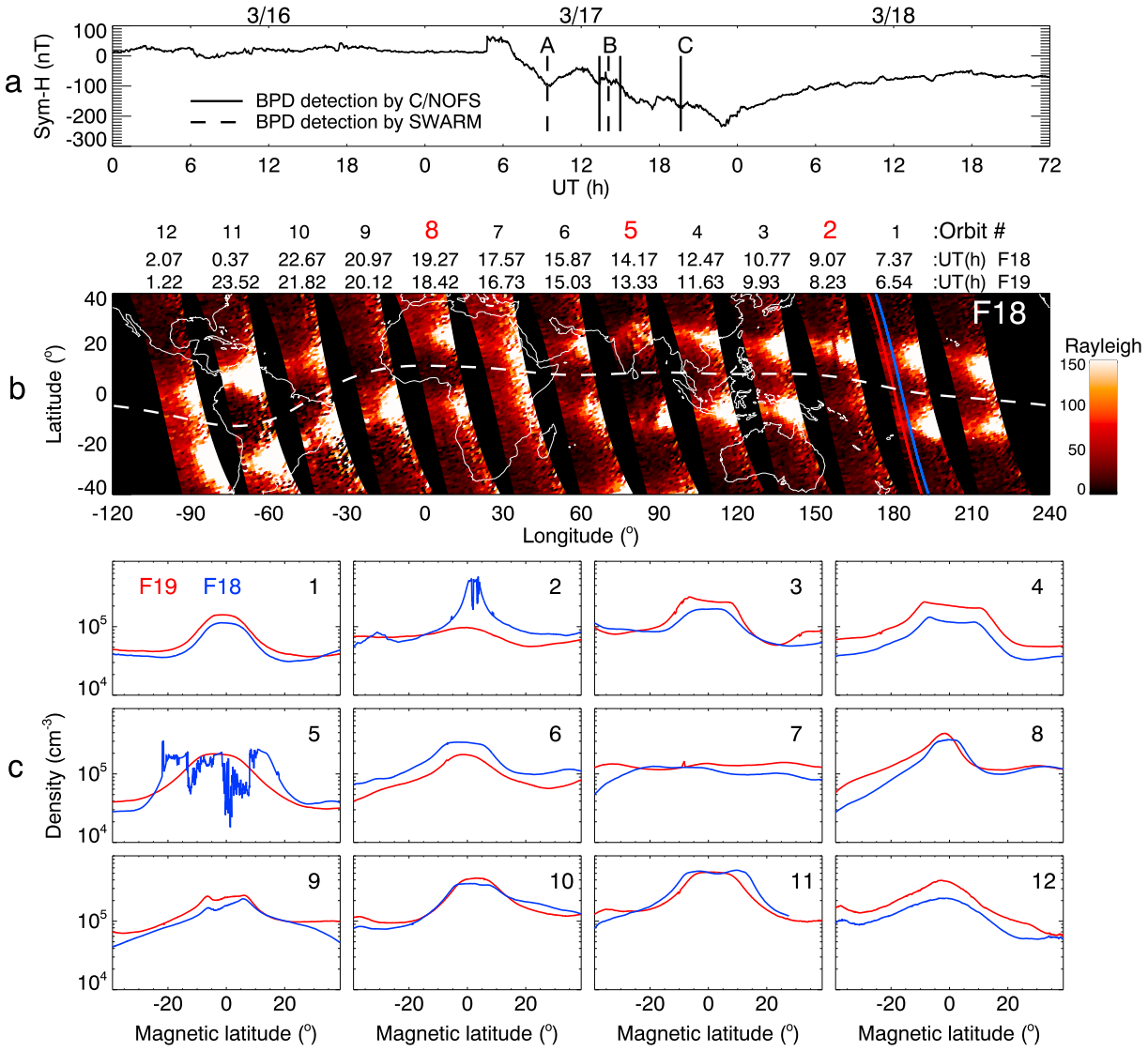

Figure 1. (a) *SYM-H* index in 16–18 March 2015 obtained from the World Data Center in Kyoto University (http://wdc.kugi.kyoto-u.ac.jp/aeasy/index.html). The times at which BPDs were detected by Swarm and C/NOFS satellites are indicated by the vertical dashed and solid lines, respectively. (b) Composite DMSP F18/SSUSI OI 135.6 nm image on 17 March 2015. The red and blue lines are the ground tracks of DMSP F19 and F18, respectively. The UTs at which the DMSP satellites crossed the equator from south to north are given in the top. The white dashed line indicates the magnetic equator. The orbit numbers 2, 5, and 8 indicate the longitudes where BPDs were detected. (c) Comparison of the observations of the ion density by F19 (red) and F18 (blue).

22 November 2013. Swarm-Alpha (SwA) and Swarm-Charlie (SwC) pairs have orbits around an altitude of 460 km with a separation of about 75 km in geographic latitude and about 150 km in geographic longitude. Swarm-Bravo (SwB) has an orbit around an altitude of 530 km. The orbital inclinations of SwA and SwC pairs and SwB are 87.4° and 88°, respectively. Our study uses the measurements of the electron density at a sampling period of 0.5 s by the Langmuir probes.

3. Results

3.1. Overview of the Equatorial Ionosphere Disturbance During the Storm

Figure 1 provides an overview of the ionospheric variations during the main phase of the 17 March 2015 storm. The *SYM-H* index in Figure 1a represents the geomagnetic disturbances of the horizontal magnetic field component (*H*) in midlatitudes. The main phase of the storm started around 6 h universal time (UT) following the turning of the interplanetary magnetic field southward. *SYM-H* reached a minimum value of

−234 nT at 22.8 h UT. BPDs were detected around 9.4, 14.1, and 19.8 h UTs. The vertical lines on the *SYM-H* index indicate the detection times of BPDs by the Swarm (dashed lines) and C/NOFS (solid lines) satellites. Figure 1b shows the composite swaths of the F18/SSUSI OI 135.6 nm intensity. The ground track of a single pass of F18 is shown with a blue line on the swath of orbit 1 of that day. The UTs at which F18 crossed the geographic equator are given in the top of Figure 1b (7.37 h UT for the marked pass of F18). A single pass of F19 is also shown with a red line on the swath of orbit 1, and the UTs of F19 passes are given in the top (6.54 h UT for the marked pass of F19). F19 and F18 sampled similar longitude regions with an interval of 50 min. To show the variation of the ionosphere at the evening terminator, the observations of plasma density by F19 (18.6 h LT) and F18 (19.6 h LT) are compared in Figure 1c.

BPDs were detected by C/NOFS or Swarm in the longitudes of DMSP passes 2, 5, and 8. Bubbles were detected by Swarm and DMSP in the longitudes of DMSP passes 2 and 5, but no bubble was detected in the longitude of DMSP pass 8 by any satellite. Thus, the BPD in the longitude of DMSP pass 8 has nothing to do with bubbles. C/NOFS detected bubbles in the longitude of DMSP pass 6 as well as in the longitudes of DMSP passes 2 and 5. Comparing the F19 and F18 observations in Figure 1c, the longitudes of DMSP passes 2, 5, and 6 are distinguished from other regions by the observation of higher plasma density in the F18 orbits than in the F19 orbits. Therefore, bubbles occurred in the longitudes where the plasma density increased between 18.6 h (F19) and 19.6 h (F18) LT. Because the PRE typically has its peak value in this LT interval [*Kil et al*., 2009a], the PRE is a plausible source of the plasma density enhancements and the occurrence of bubbles in those longitudes. The occurrence of both BPDs and bubbles in the longitudes of DMSP passes 2 and 5 may indicate the association of BPDs with the PRE and bubbles. The equatorial ionization anomaly (EIA) is most pronounced in the Atlantic sector (longitude of DMSP pass 11) in the SSUSI image. The EIA feature is also visible in the F18/SSIES data in that longitude. However, bubbles did not develop in that region. Judging from the ionospheric morphology in Figure 1c, the onset of bubbles is seen to be affected by the magnitude of the ionospheric change (enhancement in vertical plasma motion or plasma density) at the terminator rather than by the EIA intensity which was produced before the PRE. In the following sections, we closely look at the observations in the longitudes where BPDs were detected.

3.2. A BPD at the Longitude of 155°E

SwC detected a Type 2 BPD, and C/NOFS detected bubbles at 155°E longitude (DMSP pass 2 in Figure 1b). Figure 2 presents the coincident observations of the ionosphere in that region. The DMSP F18/SSUSI OI 135.6 nm image is shown in Figure 2a with the ground tracks of Swarm, DMSP F18, and C/NOFS satellites. The thick yellow lines in the SwA and SwB orbits indicate the detection locations of plasma depletions in those orbits. The colors of the satellite ground tracks match the colors of their observations. The same OI 135.6 nm image is shown again in Figure 2b for a clearer view. The observations of F18/SSIES, SwA, and SwC are shown in Figures 2c–2e, and their orbit information is given in Figure 2h. Because SwA and SwC flew near each other, the orbit information is given only for SwC. The C/NOFS orbit information and C/NOFS observations are given in Figures 2f and 2g, respectively.

The F18 observations were made around 9.1 h UT. An emission depletion band appears in the SSUSI image (Figure 2b), and plasma depletions appear in the equatorial region in the SSIES data (Figure 2c). The vertical velocity is shown with black dots in Figure 2c. A pronounced density enhancement occurs in the equatorial region, and this enhancement agrees well with the enhancement in the vertical ion velocity. In Swarm observations (Figures 2d and 2e), four depletions (A–D) appear. Among these depletions, depletion D in the SwC orbit is most pronounced. Its latitudinal width is about 15° and the plasma density is lower than the ambient plasma by more than a factor of 1000. We call this depletion a Type 2 BPD. The steep density gradient at the walls of the BPD is different from the morphology of the equatorial ionization trough that normally shows a gradual density variation as a function of latitude. Thus, the formation of the BPD is not explained simply by the uplift of the background ionosphere. In the SSUSI image, we can identify a tilted emission depletion band at the longitude of 150°–160°E. A tilted bubble is produced by the differential zonal drift of plasma-depleted magnetic flux tubes and has a shell structure [*Kil et al*., 2009b]. The detection longitude of the shell structure varies with latitude and altitude. Given the appearance of the single pronounced emission depletion band at the locations of the plasma depletions in the DMSP and Swarm orbits, it is reasonable to suggest that the plasma depletions and the emission depletion band are associated with the same bubble.

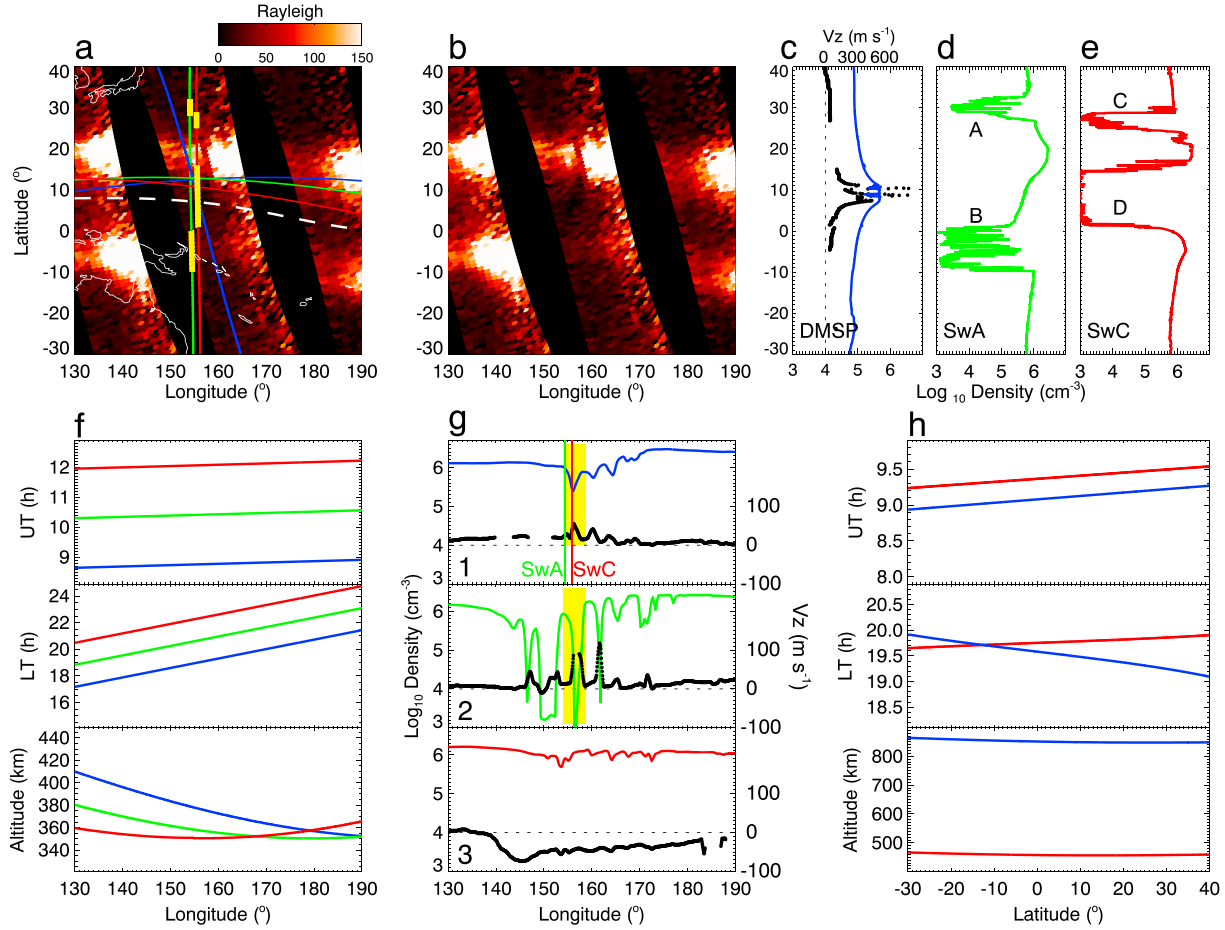

Figure 2. DMSP F18, Swarm, and C/NOFS observations in the longitude of 130°–190°E. (a) SSUSI OI 135.6 nm image with satellite passes. (b) SSUSI OI 135.6 nm image. (c–e) Plasma density observed by F18, SwA, and SwC. The vertical ion velocity observed by F18 is shown with black dots in Figure 2c. (f) UT, LT, and altitude of C/NOFS orbits. (g) Plasma density (colored lines) and meridional component of the plasma velocity (black dots) observed by C/NOFS. The vertical green and red lines in orbit 1 indicate the longitudes of the SwA and SwC orbits, respectively. The bubble that is considered to be responsible for the emission depletion in Figure 2b is indicated with a yellow shaded area. (h) UT, LT, and altitude of F18 and SwC orbits.

The C/NOFS observations of the ion density (colored lines) and the meridional (vertical) component of the ion velocity (black dots) are shown in Figure 2g. C/NOFS orbit 1 detected depletions in the longitude of 150°–170°E at 19–20 h LT (8.8 h UT). The upward plasma motion of 20–60 m s^{-1} was observed at the locations of the plasma depletions, but the upward velocity of the background ionosphere was less than 20 m s^{-1}. In C/NOFS orbit 2 (10.4 h UT), depletions were detected over a broader range of longitudes and the depletions had deepened. The vertical motion of the background ionosphere was near zero in orbit 2. Considering the detection of shallow depletions in orbit 1 and deep depletions in orbit 2, it appears that bubbles had just started their development at the time of orbit 1. The longitudes of SwA and SwC orbits are indicated with vertical lines in Figure 2g. The depletion indicated by the yellow shaded area is likely the source of the emission depletion band in the SSUSI image and the depletions in the DMSP and Swarm orbits. Depletions had almost disappeared in the C/NOFS data by orbit 3, although orbit 3 sampled the ionosphere at lower altitudes than did orbit 2. The downward motion of the ionosphere might have caused a rapid decay of the depletions. The upward ion velocity of the background ionosphere was small in the C/NOFS orbit 1 (8.8 h UT), but it increased significantly (>100 m s^{-1}) in the F18 orbit (9.1 h UT). Thus, the F18 observations were made within 20 min after the significant uplift had started. The enhancement of the equatorial plasma density in the F18 orbit would be because the observation was made during the time when there was a rapidly increasing uplift of the ionosphere.

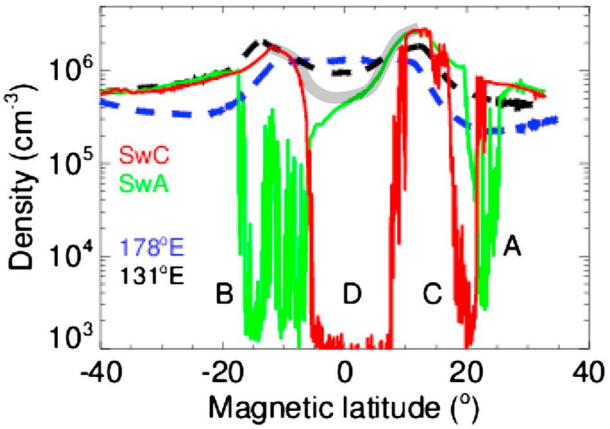

Figure 3. Comparison the SwA (green) and SwC (red) observations in Figure 2 along with the SwA observations at the longitudes of 178°E (blue) and 131°E (black).

The locations of depletions A and C in the Swarm observations correspond to the location of the emission depletion band in the middle SSUSI swath. The detection of depletion A at a higher latitude than depletion C is consistent with the westward tilt of the emission depletion band. The longitudes of the magnetic apex of depletions A and C correspond to the longitudes of the depletions detected by DMSP near the magnetic equator. The detection latitudes of the depletions in Swarm observations are puzzling because the locations of the depletions are not symmetric with respect to the magnetic equator. The observations of SwA (green) and SwC (red) near 155°E longitude are shown in Figure 3. For comparison, the SwA observations near the longitudes of 178°E (blue) and 131°E (black) are also shown with dashed lines. There is no depletion at the southern conjugate location of depletion C. The sizes and locations of depletions A and B do not match either. We postpone the discussion of the morphology of depletions to section 4. Ignoring the plasma-depleted regions in the green and red curves, we can see almost an identical latitudinal morphology of the background ionosphere. This observation indicates that the appearance of a BPD only in the SwC orbit is not related to the modulation of the background ionosphere. By combining the two observations, we can infer the morphology of the background ionosphere at the location of the BPD. The gray thick curve schematically illustrates the morphology of the trough in that longitude. Additional plasma depletion mechanisms are necessary to explain the density difference between the trough and the BPD. A stronger EIA and a deeper trough developed near 155°E longitude than in the neighboring longitudes (dashed curves). However, the uplift of the background ionosphere near the longitude of 155°E was not so severe as to move the whole *F* region above C/NOFS orbits (~350 km) because a BPD feature did not appear in the C/NOFS observations. If the BPD was not produced by the uplift of the background ionosphere, the BPD is likely associated with a bubble. We interpret that the BPD in the SwC orbit represents the elongated nature of bubbles along the magnetic field lines. Because the longitudinal cross section of a bubble (C/NOFS orbit) is narrower than its latitudinal cross section (SwC orbit), the BPD feature is not obvious in the C/NOFS orbit.

3.3. BPDs in the Longitude of 70°–90°E

The longitude of 70°–90°E (DMSP pass 5 in Figure 1b) is the region where BPDs and bubbles were detected by both Swarm and C/NOFS. The intensification of the EIA in the F18 orbit compared with the observation in the F19 orbit (see orbit 5 in Figure 1c) indicates that the ionospheric uplift was significant in the evening. The uplift can also be identified from the measurements of the ion velocity. Figure 4 is the same format as Figure 2 for the observations in the longitude of 50°–120°E. Because SwA and SwC detected similar BPDs, we present SwB observations in the region instead of SwC observations.

Multiple bubble features appear in the middle SSUSI swath (Figure 4b). In the equatorial region, the background emission intensity in the middle swath is lower than that in neighboring longitudes. These observations lead to the interpretation that the PRE was significant around the longitude of 70°–90°E and bubbles developed in association with the PRE. SwA detected a Type 2 BPD in that region at 14.1 h UT (Figure 4c). The BPD has steep walls and a flat bottom with a latitudinal width of 17°. F18 (14.2 h UT) and SwB (16.3 h UT) detected irregularities, but deep depletions do not appear in those orbits (Figures 4d and 4e). The vertical plasma motion is visible at some disturbed locations at the time of the F18 observation, but the background ionosphere does not show a notable upward motion. Considering the observation of an intense upward motion of the background ionosphere at the same LT in the longitude of 150°–160°E (Figure 2c), the PRE seems to have ended earlier in the longitude of 70°–90°E than in the longitude of

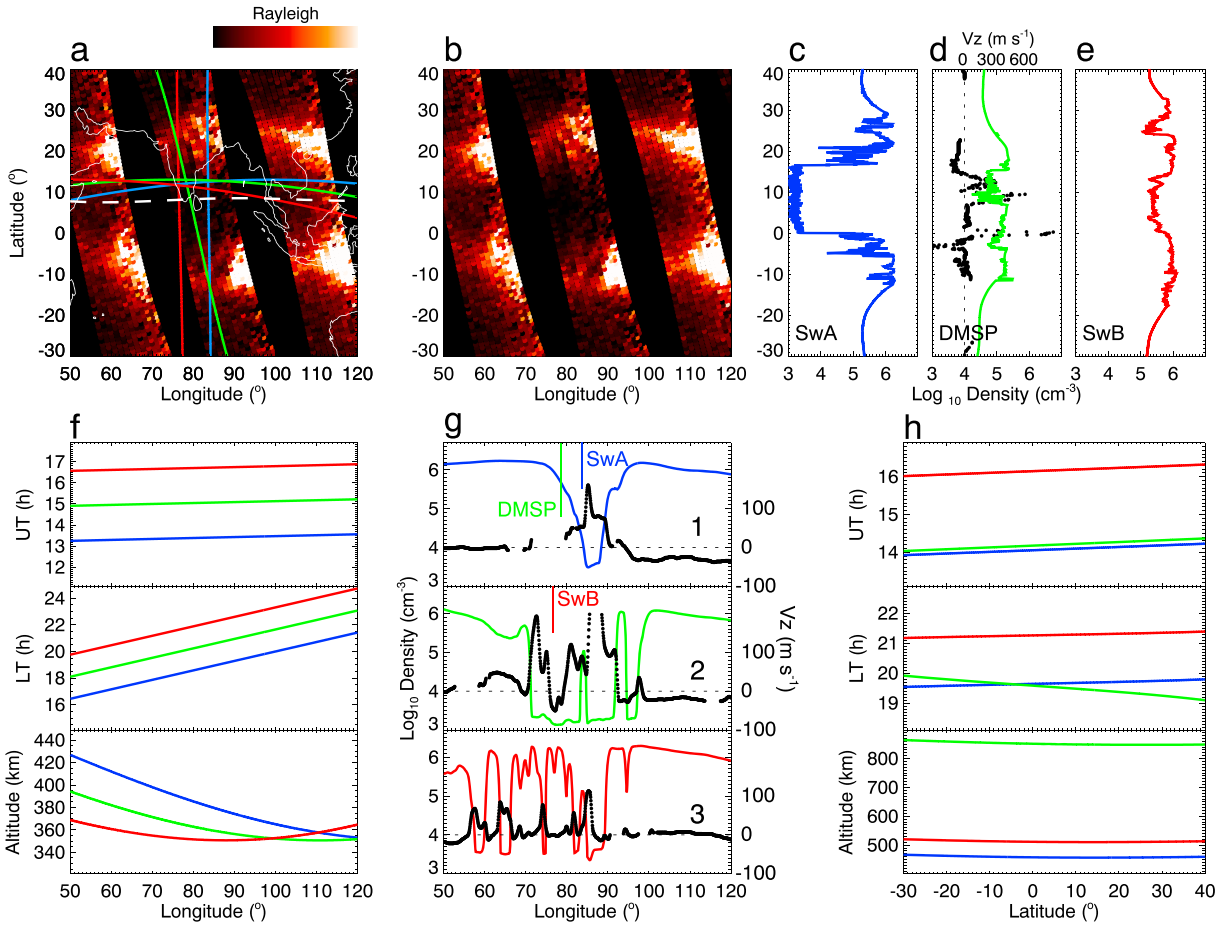

Figure 4. The same format as Figure 2 for the observations in the longitude of 50°–120°E.

150°–160°E. The absence of the EIA feature in Figure 2c (150°–160°E) and the development of a strong EIA feature in Figure 4d (70°–90°E) are attributed to the difference in the occurrence times of the PRE.

In Figure 4g, a single large depletion appears in C/NOFS orbit 1 at 13.5 h UT (19 h LT), and we call this depletion a Type 1 BPD. 19 h LT is the time at which PRE reaches near its peak value under normal conditions. Because this time is a little bit early for the onset of bubbles and the depletion is much broader than regular bubbles, the BPD is not interpreted as a bubble. In addition, the gradual density variation is not the characteristic of a bubble. In C/NOFS orbit 2 at 15.0 h UT, two depletions with the longitudinal widths of 12° (near 75°E) and 7° (near 90°E) are categorized as Type 2 BPDs. A Type 2 BPD feature also exists near the longitude of 88°E in C/NOFS orbit 3.

Ionospheric disturbances in this longitude region (Indian sector) were reported by *Ramsingh et al.* [2015] and *Tulasi Ram et al.* [2016]. Both studies identified the ionospheric uplift over India at 13.5–14.0 h UT from the ionosonde observations at Tirunelveli (longitude: 77.7°E, latitude: 8.7°N) and attributed this phenomenon to the action of a penetration electric field at the dusk sector. The ground-based observations in India are consistent with the observations of the upward plasma motion by C/NOFS (Figure 4g), the appearance of an EIA feature in the DMSP F18 orbit (Figure 4d), and the development of an equatorial ionization trough in the SwB orbit (Figure 4e). *Tulasi Ram et al.* [2016] reported that spread *F* started to appear over Tirunelveli after 13.9 h UT. Because the observations in C/NOFS orbit 1 were made before the spread *F* onset, the BPD in C/NOFS orbit 1 is not related to a bubble, as we described above. The uplift of the ionosphere by the PRE is likely to be the source of the BPD in C/NOFS orbit 1. The gradual density variation at the walls of the Type 1 BPD in C/NOFS orbit 1 is different from the steep density gradient at the walls of the Type 2 BPDs in C/NOFS orbit 2. The observations in C/NOFS orbit 2 were made after the development of bubbles in the

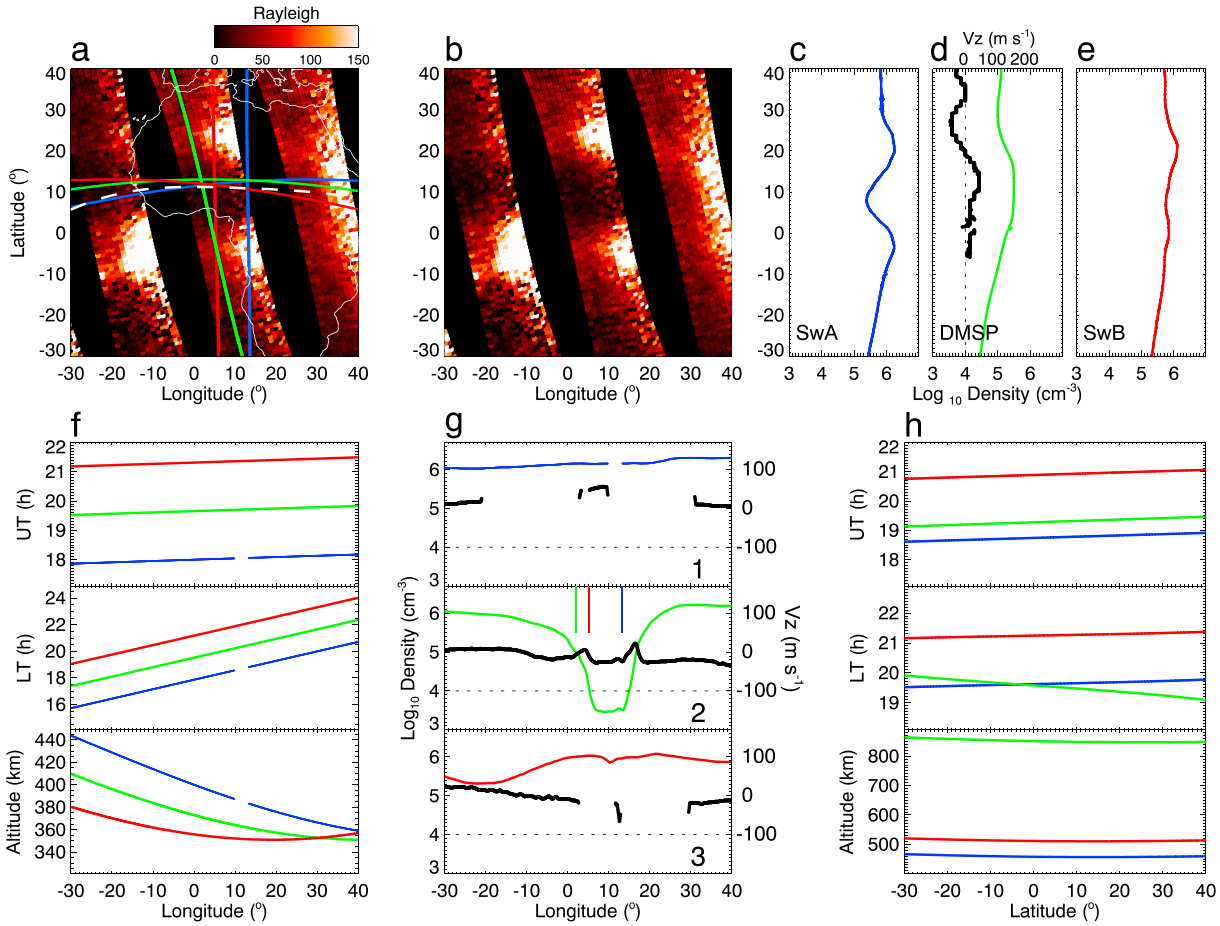

Figure 5. The same format as Figure 2 for the observations in the longitude of 30°W–40°E.

region. These observations provide a clue for the morphology of BPDs associated with the PRE and bubbles. The Type 1 BPD associated with the PRE has a gradual density variation like the one in C/NOFS orbit 1, whereas the Type 2 BPD accompanied with bubbles has steep walls like the ones in C/NOFS orbit 2. The absence of a BPD feature in the DMSP and SwB observations may reflect the altitude dependence of the detection of BPDs.

The development of a strong PRE over India during the main phase of the storm is evident by our observations and previous studies. The virtual height obtained from the ionosonde observations at Tirunelveli reached over 550 km at 14 h UT [*Ramsingh et al.*, 2015; *Tulasi Ram et al.*, 2016]. *Joshi et al.* [2016] conducted SAMI2 (Sami2 is another model of the ionosphere) model simulations using the vertical plasma drift data at Tirunelveli. Their results showed that the *F* peak height reached over 500 km just after the PRE. Therefore, the SwA orbit (470 km) was likely below the *F* peak height at the time of the BPD detection. However, the morphology of the BPD is difficult to explain by the effect of the PRE alone because the uplift itself does not create such a steep latitudinal density gradient. The steep density gradient indicates that SwA encountered a discontinuity in density. Bubbles are the likely source of the discontinuity.

3.4. A BPD at the Longitude of 10°E

At 10°E longitude (DMSP pass 8 in Figure 1b), a Type 1 BPD was detected by C/NOFS, but no bubble was detected by any satellites. The absence of bubbles distinguishes this region from the other two regions described in sections 3.2 and 3.3. Figure 5 is the same format as Figure 4 for the observations at 30°W–40°E longitude. The EIA and trough are clearly visible in the SwA orbit at 18.8 h UT (Figure 5c). The density has its peak value in the equatorial region in the DMSP F18 orbit at 19.3 h UT (Figure 5d), and weak features of the EIA and trough appear in the SwB orbit at 20.9 h UT (Figure 5e). These are typical ionospheric

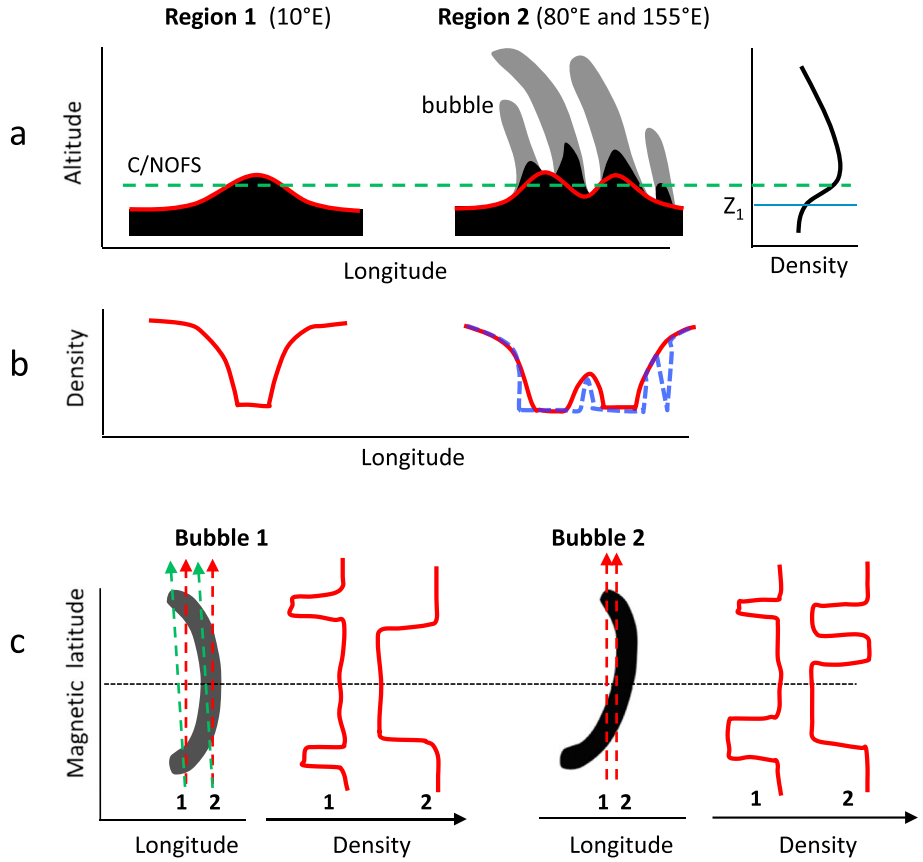

Figure 6. Schematic illustration of the BPD morphology. (a) Modulation of the background ionosphere in the absence (Region 1) and presence (Region 2) of bubbles. The red curves represent the bottom (Z_1) of the *F* region. (b) Longitudinal density profiles along the C/NOFS orbit. In Region 2, the presence of bubbles makes the walls of BPDs steep (blue dashed line). (c) Bubble images projected in the longitude-latitude plane and the bubble morphology along polar orbit satellite passes. See the text for the details.

morphologies at the altitudes of those satellites under normal conditions. The vertical ion velocity in the equatorial region was 10–40 m s^{-1} at the time of the F18 observations.

In C/NOFS orbit 1 at 18 h UT (Figure 5g), the density does not show any notable longitudinal variation. The vertical ion velocity at the longitude of 2°–10°E is about 50 m s^{-1}. We are not able to identify whether the upward plasma motion was confined to the longitude of 2°–10°E because of the data gap. A BPD appears near 10°E longitude in C/NOFS orbit 2 at 19.7 h UT. The SwA (blue), F18 (green), and SwB (red) orbits are indicated with vertical lines. The morphology of this BPD is similar to that of the BPD in C/NOFS orbit 1 in Figure 4g; both BPDs show a gradual density variation at the walls and have a flat bottom.

In the SSUSI image in Figure 5b, the EIA is more pronounced in the middle swath than in other swaths. We also identified the development of stronger EIA and trough near 10°E longitude than in nearby longitudes from Swarm observations (not shown). Therefore, the uplift near 10°E longitude was more significant than in neighboring longitudes. However, the uplift in this region was not as strong as that in the other two regions described in sections 3.2 and 3.3, judging from the latitudinal morphology of the ionosphere in those regions. Bubbles might have not developed in 10°E longitude region because the PRE was not intense. This isolated BPD event provides a good reference for the morphology of a BPD in the absence of bubbles.

4. Interpretation of the BPD Morphology

We explain the morphology of the BPDs observed in the three longitude regions using the diagrams in Figure 6. The diagrams in Figure 6a illustrate the longitudinal variation of the heights of the *F* region in

two regions where bubbles are absent (Region 1) and present (Region 2). The vertical electron density profile is shown on the right of Region 2. The red lines in Region 1 and Region 2 indicate the bottom (Z_1) of the *F* region in the density profile. The C/NOFS orbit (green dashed line) is assumed to be along the magnetic equator. The density profiles along the C/NOFS orbit are shown in Figure 6b. The gradual density variation in Region 1 represents the density profile in the bottomside, and the flat density at the bottom of the depletion is related to the sampling of the ionosphere below Z_1. The diagrams in Region 1 may explain the BPDs in C/NOFS orbit 1 in Figure 4g and C/NOFS orbit 2 in Figure 5g. In Region 2, the C/NOFS orbit passes through two humps in the *F* region height. The density profile associated with the humps is depicted by the red curve. The two humps can be produced, if the strength of the penetration electric field varies with time (or longitude) or a seeding mechanism modulates the bottomside. In the presence of bubbles, the BPDs become broader and have steep walls as illustrated with the blue dashed curve [e.g., *Lee et al*., 2014]. This diagram may explain the BPDs in C/NOFS orbit 2 in Figure 4g.

The diagrams in Figure 6c describe two-dimensional bubble images in the longitude-latitude coordinates and the latitudinal density profiles along the satellite orbits. Bubble 1 is a snapshot of a bubble at a certain UT. The bubble is symmetric with respect to the magnetic equator. The magnetic declination is assumed to be zero. If we sample the ionosphere simultaneously along the red dashed lines, the morphology of the depletion is symmetric with respect to the magnetic equator. However, bubbles are not stationary and satellite observations are not a snapshot. If the bubble drifts eastward, the satellite actually samples the bubble along the passes shown with green dashed lines. The slant angle depends on the drift velocity of the bubble and the satellite velocity. The rotation of the Earth and positive magnetic declination further increase the slant angle. Thus, a symmetric bubble appears to be a slanted bubble (Bubble 2) when it is viewed along the satellite pass. The latitudinally asymmetric distribution of depletions in Swarm observations in Figure 2 may be explained by this picture of a slanted bubble. Orbits 1 and 2 in Bubble 2 represent the orbits of SwA and SwC. The depletions along these orbits are asymmetric. In addition to the effects of magnetic declination and zonal motion of bubbles, the hemispheric asymmetry of the background ionosphere and temporal growth of a bubble can cause a hemispheric asymmetry in the morphology of a bubble. For example, if the northern ionosphere was lifted by equatorward winds or a northbound satellite observed a rapidly growing bubble, the satellite would have a higher chance of detecting a bubble in the Northern Hemisphere than in the Southern Hemisphere.

We note that BPDs are not confined to storm periods. Because the detection of a BPD depends on the satellite orbit (altitude and inclination), *F* region height, and occurrence of bubbles, BPDs can appear anytime when the proper conditions are met. The necessary condition for the detection of a BPD is the uplift of the bottom of the *F* region above the satellite orbits by either the modulation of the background ionosphere or the creation of bubbles. The reason that BPDs preferentially occur during storm periods is because storm-induced electric fields can provide that condition.

5. Conclusions

Abnormally large plasma depletions were detected by C/NOFS and Swarm satellites in the equatorial *F* region during the main phase of the 17 March 2015 storm. These depletions, named BPDs, were detected at the times of the development of the PRE and just after the PRE. Two different types of BPDs occurred: Type 1 BPDs had a gradual density variation and Type 2 BPDs had a steep density gradient at the walls. The Type 1 BPDs did not accompany bubbles, whereas the Type 2 BPDs accompanied bubbles. The detection of the Type 1 BPD is attributed to the uplift of the *F* region above satellite altitudes by the PRE. The detection of the Type 2 BPDs is associated with the spatial discontinuity of the ionosphere in the region where the ionosphere is lifted. Bubbles are responsible for the spatial discontinuity. The appearance of bubbles in polar orbit satellites can be asymmetric in hemisphere due to many factors including the zonal motion of bubbles, rotation of the Earth, magnetic declination, and the hemispheric asymmetry of the background ionosphere. Our results will be helpful in the interpretation of various forms of depletions in Swarm and C/NOFS observations.

Acknowledgments

H. Kil acknowledges the support from the Stuart S. Janney Publication Program in JHU/APL. This work was also supported by Korea Polar Research Institute (PE16090) and Wright-Patterson Air Force Base. W.K. Lee acknowledges support from basic research funds from the Korea Astronomy and Space Science Institute (2016-1-85302). The work by M.R. Hairston was supported by NASA grant NNX15AT31G and NSF grant Ags-1552245. The authors acknowledge the Swarm team for the Swarm data in the website (https://earth.esa.int/web/guest/missions/esa-operational-eo-missions/swarm). The DMSP and C/NOFS data are available by contacting H. Kil (hyosub.kil@jhuapl.edu).

References

Basu, S., et al. (2001), Ionospheric effects of major magnetic storms during the International Space Weather Period of September and October 1999: GPS observations, VHF/UHF scintillations, and in situ density structures at middle and equatorial latitudes, *J. Geophys. Res.*, *106*(A12), 30,389–30,413, doi:10.1029/2001JA001116.

Basu, S., S. Basu, F. J. Rich, K. M. Groves, E. MacKenzie, C. Coker, Y. Sahai, P. R. Fagundes, and F. Becker-Guedes (2007), Response of the equatorial ionosphere at dusk to penetration electric fields during intense magnetic storms, *J. Geophys. Res.*, *112*, A08308, doi:10.1029/2006JA012192.

Burke, W. J., A. G. Rubin, N. C. Maynard, L. C. Gentile, P. J. Sultan, F. J. Rich, O. de La Beaujardière, C. Y. Huang, and G. R. Wilson (2000), Ionospheric disturbances observed by DMSP at middle to low latitudes during the magnetic storm of June 4–6, 1991, *J. Geophys. Res.*, *105*(A8), 18,391–18,405, doi:10.1029/1999JA000188.

Burke, W. J., O. de La Beaujardière, L. C. Gentile, D. E. Hunton, R. F. Pfaff, P. A. Roddy, Y.-J. Su, and G. R. Wilson (2009), C/NOFS observations of plasma density and electric field irregularities at post-midnight local times, *Geophys. Res. Lett.*, *36*, L00C09, doi:10.1029/2009GL038879.

de la Beaujardière, O., and The C/NOFS Definition Team (2004), C/NOFS: A mission to forecast scintillations, *J. Atmos. Sol. Terr. Phys.*, *66*, 1573, doi:10.1016/j.jastp.2004.07.030.

Greenspan, M. E., C. E. Rasmussen, W. J. Burke, and M. A. Abdu (1991), Equatorial density depletions observed at 840 km during the great magnetic storm of March 1989, *J. Geophys. Res.*, *96*(A8), 13,931–13,942, doi:10.1029/91JA01264.

Heelis, R. A., W. R. Coley, A. G. Burrell, M. R. Hairston, G. D. Earle, M. D. Perdue, R. A. Power, L. L. Harmon, B. J. Holt, and C. R. Lippincott (2009), Behavior of the O^+/H^+ transition height during the extreme solar minimum of 2008, *Geophys. Res. Lett.*, *36*, L00C03, doi:10.1029/2009GL038652.

Huang, C.-S., O. de La Beaujardiere, P. A. Roddy, D. E. Hunton, R. F. Pfaff, C. E. Valladares, and J. O. Ballenthin (2011), Evolution of equatorial ionospheric plasma bubbles and formation of broad plasma depletions measured by the C/NOFS satellite during deep solar minimum, *J. Geophys. Res.*, *116*, A03309, doi:10.1029/2010JA015982.

Huang, C.-S., J. M. Retterer, O. de La Beaujadiere, P. A. Roddy, D. E. Hunton, J. O. Ballenthin, and R. F. Pfaff (2012), Observations and simulations of formation of broad plasma depletions through merging process, *J. Geophys. Res.*, *117*, A02314, doi:10.1029/2011JA017084.

Huba, J. D., T.-W. Wu, and J. J. Makela (2015), Electrostatic reconnection in the ionosphere, *Geophys. Res. Lett.*, *42*, 1626–1631, doi:10.1002/2015GL063187.

Joshi, L. M., S. Sripathi, and R. Singh (2016), Simulation of low-latitude ionospheric response to 2015 St. Patrick's Day super geomagnetic storm using ionosonde-derived PRE vertical drifts over Indian region, *J. Geophys. Res. Space Physics*, *121*, 2489–2502, doi:10.1002/2015JA021512.

Kelley, M. C. (2009), *The Earth's Ionosphere: Plasma Physics and Electrodynamics*, vol. 96, 2nd ed., Academic Press, Burlington, Mass.

Kil, H., and W. K. Lee (2013), Are plasma bubbles a prerequisite for the formation of broad plasma depletions in the equatorial *F* region?, *Geophys. Res. Lett.*, *40*, 3491–3495, doi:10.1002/grl.50693.

Kil, H., and L. J. Paxton (2006), Ionospheric disturbances during the magnetic storm of 15 July 2000: Role of the fountain effect and plasma bubbles for the formation of large equatorial plasma density depletions, *J. Geophys. Res.*, *111*, A12311, doi:10.1029/2006JA011742.

Kil, H., L. J. Paxton, S.-Y. Su, Y. Zhang, and H. Yeh (2006), Characteristics of the storm-induced big bubbles (SIBBs), *J. Geophys. Res.*, *111*, A10308, doi:10.1029/2006JA011743.

Kil, H., S.-J. Oh, L. J. Paxton, Y. Zhang, S.-Y. Su, and K.-W. Min (2007), Spike-like change of the vertical $\mathbf{E} \times \mathbf{B}$ drift in the equatorial region during very large geomagnetic storms, *Geophys. Res. Lett.*, *34*, L09103, doi:10.1029/2007GL029277.

Kil, H., S.-J. Oh, and L. J. Paxton (2008), Abnormal vertical drifts of equatorial plasma before dawn and after sunset during the storm of October 29–30, 2003, *Geophys. Res. Lett.*, *35*, L19106, doi:10.1029/2008GL035643.

Kil, H., S.-J. Oh, L. J. Paxton, and T.-W. Fang (2009a), High-resolution vertical drift model driven from the ROCSAT-1 data, *J. Geophys. Res.*, *114*, A10314, doi:10.1029/2009JA014324.

Kil, H., R. A. Heelis, L. J. Paxton, and S.-J. Oh (2009b), Formation of a plasma depletion shell in the equatorial ionosphere, *J. Geophys. Res.*, *114*, A11302, doi:10.1029/2009JA014369.

Lee, W. K., H. Kil, L. J. Paxton, Y. S. Kwak, Y. Zhang, I. Galkin, and I. S. Batista (2014), Equatorial broad plasma depletions associated with the enhanced fountain effect, *J. Geophys. Res. Space Physics*, *119*, 402–410, doi:10.1002/2013JA019137.

Lühr, H., J. Park, J. W. Gjerloev, J. Rauberg, I. Michaelis, J. M. G. Merayo, and P. Brauer (2015), Field-aligned currents' scale analysis performed with the Swarm constellation, *Geophys. Res. Lett.*, *42*, 1–8, doi:10.1002/2014GL062453.

Paxton, L. J., C. I. Meng, G. H. Fountain, B. S. Ogorzalek, E. H. Darlington, J. Goldsten, S. Geary, D. Kusnierkiewicz, S. C. Lee, and K. Peacock (1992a), Special Sensor UV Spectrographic Imager (SSUSI): An instrument description, *Proc. SPIE*, *1745*, 2–16.

Paxton, L. J., et al. (1992b), SSUSI: Horizon-to-horizon and limb-viewing spectrographic imager for remote sensing of environmental parameters, *Proc. SPIE*, *1764*, 161–176.

Ramsingh, S., S. Sripathi, S. Sreekumar, K. Banola, P. T. Emperumal, and B. S. Kumar (2015), Low-latitude ionosphere response to super geomagnetic storm of 17/18 March 2015: Results from a chain of ground-based observations over Indian sector, *J. Geophys. Res. Space Physics*, *120*, 10,864–10,882, doi:10.1002/2015JA021509.

Su, S.-Y., H. C. Yeh, C. K. Chao, and R. A. Heelis (2002), Observation of a large density dropout across the magnetic field at 600 km altitude during the 6–7 April 2000 magnetic storm, *J. Geophys. Res.*, *107*(A11), 1404, doi:10.1029/2001JA007552.

Sultan, P. J. (1996), Linear theory and modeling of the Rayleigh-Taylor instability leading to the occurrence of equatorial spread *F*, *J. Geophys. Res.*, *101*(A12), 26,875–26,891, doi:10.1029/96JA00682.

Tulasi Ram, S., et al. (2016), Duskside enhancement of equatorial zonal electric field response to convection electric fields during the St. Patrick's Day storm on 17 March 2015, *J. Geophys. Res. Space Physics*, *121*, 538–548, doi:10.1002/2015JA021932.

Woodman, R. F., and C. La Hoz (1976), Radar observations of *F* region equatorial irregularities, *J. Geophys. Res.*, *81*(31), 5447–5466, doi:10.1029/JA081i031p05447.